JOURNAL OF MATERIALS SCIENCE **38** (2003) 3965–3972

Role of magnesia and silica in alumina microstructure evolution

K. L. GAVRILOV
Enrico Fermi Institute and Department of Physics, University of Chicago, Chicago, IL 60637, USA
E-mail: klgavril@midway.ichicago.edu

S. J. BENNISON, K. R. MIKESKA
E.I. DuPont de Nemours & Co. Inc., Central Research and Development, Experimental Station, Wilmington, DE 19880-0356, USA

R. LEVI-SETTI
Enrico Fermi Institute and Department of Physics, University of Chicago, Chicago, IL 60637, USA

The effects of MgO and SiO_2 additive distributions on alumina grain morphology have been characterized using high-resolution imaging secondary ion mass spectrometry (HRI-SIMS). In alumina samples singly-doped with MgO, the concentration of Mg segregated to grain boundaries is independent of grain boundary length for a majority of grain boundaries studied. Mg segregant therefore redistributes from grain boundaries to microstructural sinks, such as pores and/or second phases, during grain coarsening. In samples singly-doped with SiO_2, abnormal grain growth develops and the concentration of Si at grain boundaries is also independent of grain boundary length. Redistribution of segregants is again necessary in this case to maintain constant grain boundary composition. Codoping with Mg/Si > 1 suppresses abnormal grain growth as a result of increased mutual solid solubility of both ions and an associated decrease in grain boundary segregation. Grain growth kinetics for doped aluminas are reconsidered in light of these observations.

1. Introduction

The influence of trace impurities used during the processing of ceramics is well known and is exploited in the control of densification, grain growth and morphology during sintering [1–4]. The ability to control microstructure is of central importance in achieving desired mechanical, electrical, magnetic and optical properties. For oxide ceramics there are two broad classes of sintering behavior determined in part by impurities and additives. At one extreme, silicate-based impurities and additives often form glassy grain boundary phases and promote elongated growth morphologies [5]. Controlled elongated grains may be desirable for certain properties such as enhanced *R*-curve (toughness) behavior [6]. If uncontrolled, these growth morphologies may develop into abnormal grains, which enlarge rapidly to many times the mean grain size, and often result in low fired densities [7] and control grain-size dependent properties, such as strength, in an unpredictable fashion [8]. At the other extreme, solid solution oxide additives with aliovalent cations of similar size to the host oxide cation may control and retard grain growth yielding high-density ceramics with uniform grain structures.

These two extremes in behavior are seen in the sintering of alumina. Studies carried out using impure alumina powders, containing uncontrolled amounts of SiO_2, Na_2O, and CaO showed abnormal grains with faceted grain morphologies and low end-point densities [7]. Experiments with controlled additions of glass-forming impurities and network modifiers have demonstrated such behavior in a more systematic fashion [5]. Coble [1, 2] established that trace additions of MgO ($\sim$0.25%) to such impure systems stabilized alumina microstructure development resulting in high end-point densities and uniform grain structures.

Many investigations have attempted to establish the underlying mechanisms that determine these two extremes in the behavior for alumina [4]. Analytical studies using techniques such as transmission electron microscopy and energy-dispersive X-ray microanalysis have shown that impurities combined with SiO_2 often form wetting grain boundary phases that control growth morphology and kinetics. Kinetic studies of densification and coarsening have been successful at identifying the phenomenological role of MgO as a grain growth suppressant [9, 10]. However, difficulties remain with assigning mechanisms to the phenomenological

descriptions of impurities and additive effects particularly for the case of MgO in alumina where MgO mitigates the effect of glassy phases. The detection of small amounts of impurities and additives in the microstructure following sintering has been a major obstacle to assigning mechanisms.

High-resolution imaging secondary ion mass spectroscopy (HRI-SIMS) techniques have recently been used to address issues of impurity/dopant detection and distribution in sintered aluminas and other ceramics [11–15]. The advantages of HRI-SIMS over other analytical techniques and conventional SIMS are: (1) a high sensitivity to trace impurities, (2) a high lateral resolution (∼50 nm), (3) an ability to sample hundreds of grains and grain boundaries in a single analysis, and (4) speed of analysis. Direct evidence for MgO segregation to grain boundaries was reported by Thompson *et al*. [14, 15] and was used to support the hypothesis that MgO suppresses grain growth through a solute drag mechanism. We have recently used high-resolution scanning SIMS to investigate MgO and SiO_2 additions to alumina [16]. The main findings of our work to date are: (1) when alumina is doped individually with MgO or SiO_2 both impurities segregate strongly to the alumina grain boundaries consistent with previous observations of Mg segregation [14, 15] and (2) MgO additions to alumina *containing* SiO_2 results in a significant redistribution of MgO and SiO_2 from the grain boundary regions into the alumina lattice. An important function of MgO is, therefore, its ability to suppress the formation of silicate-based glassy grain boundary films and significantly modify the grain boundary structure of alumina. MgO functions by increasing the mutual solid solubility of MgO and SiO_2 in bulk alumina [16]. Such changes in grain boundary structure are seen to strongly influence grain boundary sensitive properties such as the corrosion resistance of alumina to aqueous hydrofluoric acid, which is significantly improved through MgO doping [16–18]. The question remains as to how MgO and SiO_2 distributions and changes in grain boundary structure on codoping affect microstructure evolution.

In this contribution we extend our observations of MgO and SiO_2 distributions in sintered alumina using HRI-SIMS and consider the effect of dopant segregation and redistribution on grain morphology and grain growth kinetics. We confirm that MgO and SiO_2 segregate strongly to grain boundaries in alumina when added individually. Furthermore, the grain boundary concentration of these ions is not a function of grain boundary length. This observation suggests that MgO and SiO_2 segregate to a local equilibrium grain boundary concentration that is independent of grain scale and that redistribution of these dopants from boundaries to sinks occurs during coarsening. While an equilibrium thickness for siliceous grain boundaries [19] is not surprising it is an important finding for MgO segregation to grain boundaries. In light of this observation, redistribution of excess segregated impurities during coarsening should be reconsidered and may kinetically limit grain growth under certain conditions. For aluminas codoped with MgO and SiO_2, we see a reduced tendency to initiate abnormal grain growth and a total supression of abnormal grain growth when Mg/Si > 1.

2. Experimental

2.1. Materials preparation

The aluminas examined in this study were fabricated following procedures presented in detail elsewhere [16]. Sumitomo AKP-30 alumina was used as the base powder and doping was achieved by adding aliquots of various metal-salt complexes dissolved in water or ethanol followed by drying and/or hydrolyzing and deagglomeration. MgO additions were made using a $Mg(NO_3)_2{\cdot}6H_2O$ salt source (99.99% purity) and SiO_2 additions were made using a tetraethyl-orthosilicate (TEOS) source (99.99% purity). Specimens were fired in clean covered alumina crucibles containing protective powder of identical composition to the pellet. The firing schedule consisted of calcining at 1000°C for 2 h, ramping to a soak temperature of 1650°C with a specified annealing time (60–480 min). Specimens were cooled in a furnace power off condition, which gave a cooling rate on the order of 600°C/h at temperatures near the sintering temperature.

2.2. HRI-SIMS characterization

The spatial distributions of impurities and dopants in the sintered samples were characterized by high-resolution imaging secondary ion mass spectrometry (HRI-SIMS) using the instrument developed at the University of Chicago. This instrument has the unique capability of analytical image resolution of 20 nm [11]. For this experiment the microprobe was configured with a 45 keV, 25 pA Ga^+ primary ion beam extracted from a liquid metal ion source producing a 50 nm diameter probe.

Sintered alumina samples for HRI-SIMS characterization were prepared by cross sectioning and polishing to flat mirror surface finishes using successively finer grades of diamond paste down to 0.5 μm. A 3 nm gold coating was applied to the polished sections prior to HRI-SIMS microprobe imaging to eliminate charging. Images were collected after sputtering off the gold layer and any surface contamination resulting from specimen preparation. Grain boundary dopant segregation concentration estimates were made by comparing ion yields from the grain boundary regions to the grain centers, or to the near-grain boundary regions. It was assumed that matrix effects were uniform across grain boundaries. A boundary width of 1 nm was used in the calculation of grain boundary enrichment [16, 19, 20] and the estimated uncertainty in the measured values is ±20% of the mean. Further details of this instrument and its capability in analyzing ceramic and composite microstructures can be found elsewhere [11–16].

2.3. Grain morphology characterization

Scanning electron microscopy (SEM, Hitachi S-4000) was used to characterize the microstructural morphology of the sintered alumina samples. SEM samples were prepared from sintered pellets that had been

subjected to aqueous HF at 90°C, which revealed grain morphologies. After thorough washing in water and drying, the specimens were sputter-coated with a 3 nm layer of carbon to mitigate sample charging.

3. Results and discussion

3.1. MgO singly-doped alumina

Fig. 1 shows SIMS images of an alumina sample singly-doped with 500 ppm Mg/Al, sintered for 60 min at 1650°C. The induced secondary ion (ISI) map in Fig. 1a shows a flat topography with several surface polishing scratches and a small pore. The pore is located in the lower right corner of the micrograph. Fig. 1b is a SIMS map for Al^+ created using the secondary Al^+ signal from the same area in Fig. 1a. The map shows a uniform distribution of Al^+ throughout the image with the exception of two Al^+ depleted regions identified in Fig. 1b as regions 1 and 2, and a depleted region at the pores. The ratio of Al^+ signal from the alumina matrix to Al^+ signal from the depleted second phase regions is $C_{\text{alumina}}/C_{\text{second phase}} \sim 1.75$. These Al-depleted second phase regions have a high concentration of Mg as shown in the Mg^+ map in Fig. 1c. Fig. 1c shows segregation of Mg to grain boundaries and to the Mg-rich second phase regions. The enrichment ratio of Mg in the grain boundary region to Mg in the grains is, $C_{\text{gb}}/C_{\text{grain}} \sim 400$ for the processing conditions employed [16].

The increase in Mg signal from the second phase and corresponding decrease in Al signal from the second phase regions indicates that the second phase is spinel ($MgAl_2O_4$). Spinel phases have been reported in aluminas doped with trace amounts of MgO [2]. The measured ratio of 1.75 for the Al^+ signal is close to the calculated value of 1.56 based on stoichiometric alumina and $MgAl_2O_4$, assuming that the secondary Al^+ ion yields from bulk spinel and alumina are equal. Note that spinel can display significant non-stoichiometry and be present as a magnesium-deficient second phase.

Fig. 2 shows the intensity of the average Mg^+ signal along grain boundaries as a function of the grain boundary length. These data were collected from a number of Mg^+ maps including the one shown in Fig. 1c. The average Mg^+ signal is similar for all grain boundaries for the range of lengths observed. This shows a constant grain boundary concentration of Mg segregant that is independent of grain scale. It is expected that the boundaries of large grains sweep greater volumes during coarsening than small grains. For Mg

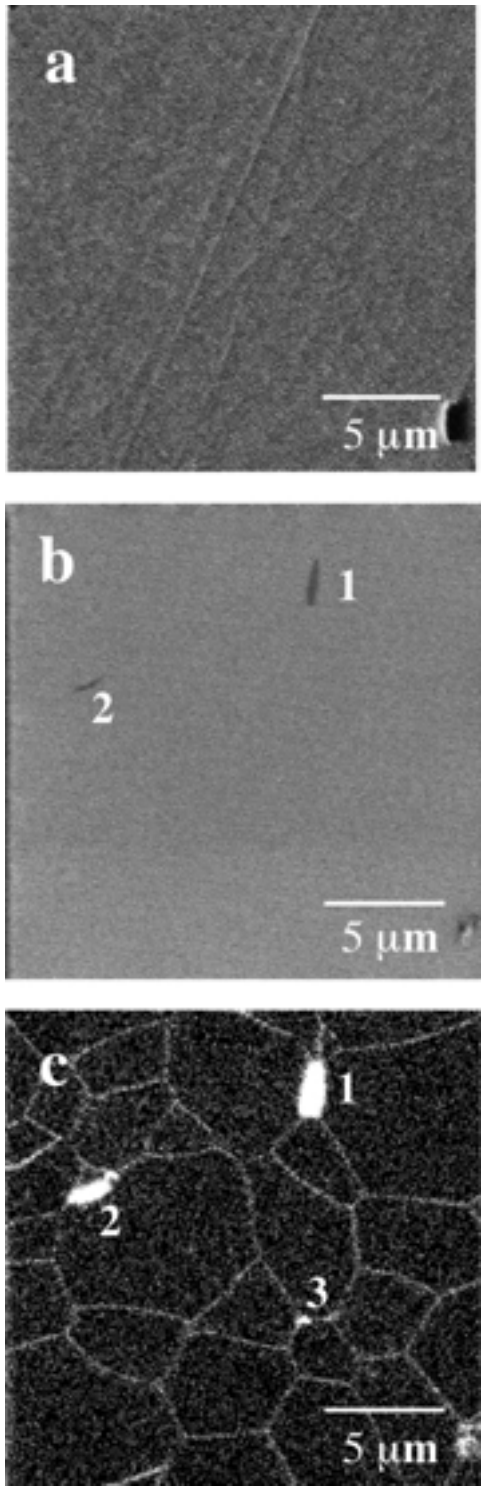

Figure 1 SIMS images of an alumina sample singly doped with MgO (Mg/Al = 500 ppm), sintered for 60 min at 1650°C. (a) ISI topographic map made using total secondary ion signal, (b) Al^+ map, and (c) Mg^+ map. Note two areas of spinel second phase denoted as location #1 and #2 on the Al^+ and Mg^+ maps.

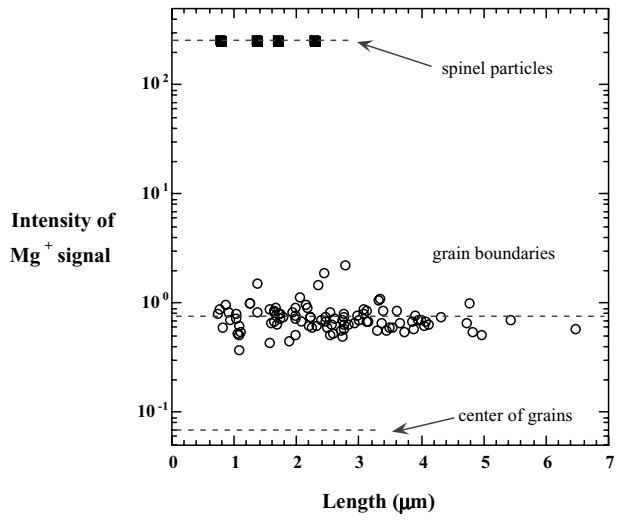

Figure 2 Mean grain boundary Mg^+ signal as a function of a grain boundary length for MgO singly-doped (Mg/Al = 500 ppm) alumina sintered for 60 min at 1650°C. Note that the concentration of Mg is independent of grain boundary length.

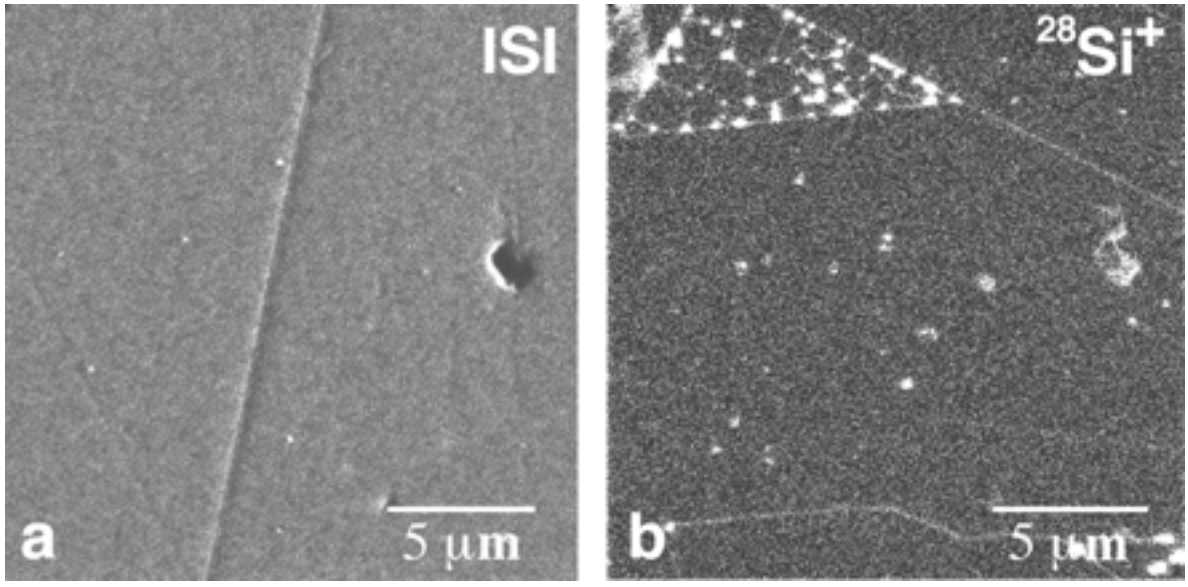

Figure 3 SIMS images of an alumina sample singly doped with SiO_2 (Si/Al = 1,000 ppm), sintered for 480 min at 1650°C. (a) ISI topographic map made using total secondary ion signal and (b) Si^+ map.

concentrations well below the solid solubility limit, Mg segregant will accumulate at grain boundaries during coarsening. Boundaries of larger grains will, therefore, show Mg^+ signals proportionally larger than signals from the boundaries of smaller grains particularly if the bulk Mg concentration is well below the solid solubility limit. Following this argument, the relative increase in Mg segregation to the grain boundaries of coarsened grain can be readily estimated by considering the dependence of grain boundary volume on scale. The largest grains seen in our study should contain grain boundaries with at least 50 times more Mg segregant than the smallest grains. In contrast to this expectation, the concentration of Mg segregant at grain boundaries was not observed to be a function of grain boundary length. This shows that there is an equilibrium grain boundary concentration of Mg and that boundaries can accommodate only a limited amount of Mg segregant.

A constant equilibrium concentration requires a considerable redistribution of excess Mg from grain boundaries to solute sinks during coarsening and will affect coarsening kinetics. During polycrystalline alumina coarsening, the total interfacial area is reduced. Since the net amount of dopant in a sample remains constant during sintering, an excess of Mg segregant over its equilibrium interfacial concentration will form in the grain boundary region as the grain boundary area decreases. Excess Mg will be transported along boundaries to sinks such as second phases and pores in the microstructure. It is interesting to note in Fig. 2 that there are a few boundaries (less than 4%) where the Mg grain boundary concentration significantly exceeds the average Mg grain boundary concentration, $C_{\text{gb-enriched}}/C_{\text{gb-average}} \sim 2.5$. These highly enriched boundaries may be precursors to spinel precipitates. We will discuss further the implications of segregant redistribution to grain coarsening kinetics in Section 3.4.

3.2. SiO_2 singly-doped alumina

Fig. 3 shows SIMS images of an alumina sample singly-doped with 1,000 ppm Si/Al, sintered for 480 min at 1650°C. The induced secondary ion (ISI) map in Fig. 3a again shows a flat topography with several surface polishing scratches and small pores. Si segregation to grain boundaries and pore surfaces is shown in Fig. 3b. The enrichment ratio of Si in the grain boundary region to Si in the grains is, $C_{\text{gb}}/C_{\text{grain}} \sim 300$ [16]. It should be noted that the $^{28}Si^+$ signal used to form these images contains a component made up of sputtered AlH^+ molecular ions that form due to a reaction between sputtered Al and residual hydrogen in the vacuum chamber and/or alumina itself. This hidden contribution to the apparent $^{28}Si^+$ signal means that the grain boundary enrichment ratio is most likely to be an underestimate of the true Si grain boundary segregation. We have solved this problem in a separate study using an ^{29}Si-enriched SiO_2 source and have shown that Si indeed segregates strongly to alumina grain boundaries and is slightly soluble in bulk alumina [16]. Fig. 3 show a number of faceted plate-like abnormal grains and areas of finer grains. Abnormal alumina grains displaying long facets typically are of {0001} orientation and are wetted by glassy grain boundary films [5, 21]. Another important observation is a strong segregation of Si to triple point junctions, especially in the areas of small grains.

Fig. 4 shows the intensity of the average Si^+ signal along grain boundaries as a function of grain boundary length. Si segregation is independent of grain boundary length similar to the case of MgO singly-doped alumina. This observation is consistent with the hypothesis that siliceous grain boundary films exist with an equilibrium thickness [19]. Si will redistribute during coarsening to maintain a grain boundary concentration that is independent of grain scale. Without a redistribution of Si during coarsening, the film thickness would increase with grain scale and result in a greater Si^+ signal intensity in the SIMS measurement, which was not

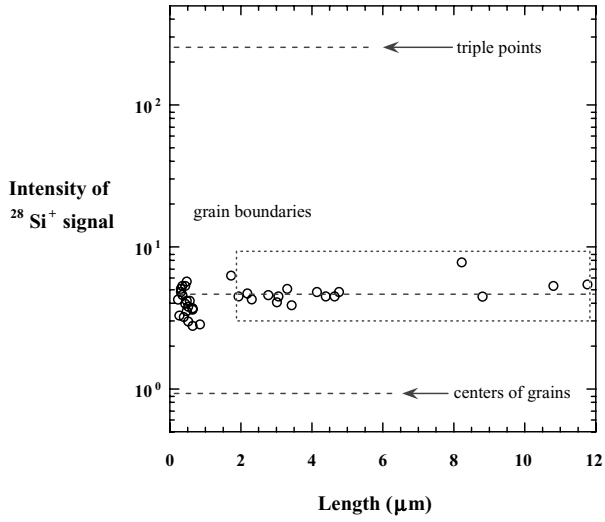

Figure 4 Mean grain boundary Si^+ signal as a function of a grain boundary length for SiO_2 singly doped alumina (Si/Al = 1000 ppm) sintered for 480 min at 1650°C. Note that the concentration of Si is independent of grain boundary length.

observed. Indeed for the range of grain sizes shown for SiO_2 singly-doped samples, the expected Si^+ signal intensity for the largest grains would be 10^4 times greater than for the smallest grains. This result shows that, similar to the case of MgO singly-doped alumina, an equilibrium concentration of Si exits at grain boundaries in alumina. Excess Si over this equilibrium concentration is accommodated by transport of the glassy phase along grain boundaries to second phase sinks, such as pores and triple points, during coarsening. Evidence of Si in triple points and pores is shown in Fig. 3b.

3.3. MgO and SiO_2 codoped alumina

Fig. 5 shows SEM micrographs for aluminas codoped with a constant concentration of 500 ppm MgO and increasing amounts of SiO_2. The figure shows uniform microstructures for Si/Mg ratios less than unity, and nonuniform abnormal grains for Si/Mg ratios greater than unity. Fig. 6 plots critical Si and Mg concentrations

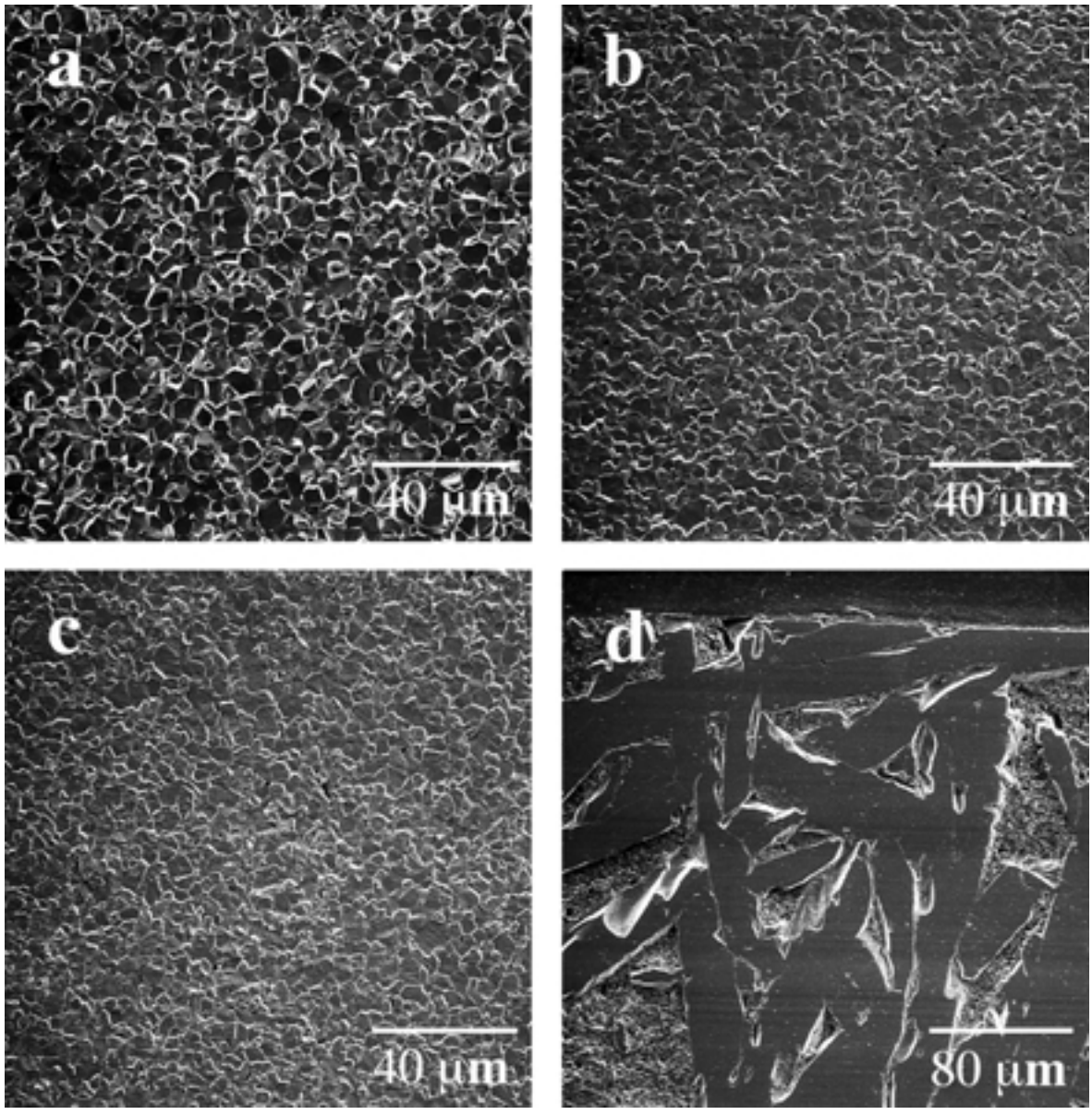

Figure 5 SEM micrographs of polycrystalline alumina doped with constant Mg/Al = 500 ppm and increasing amounts of SiO_2. The samples were etched in aqueous HF: (a) Si/Al = 0 ppm, (b) Si/Al = 250 ppm, (c) Si/Al = 500 ppm, and (d) Si/Al = 1000 ppm. For sample (d) note abnormal grains and eroded regions of small grains. A high density of Si-rich triple points in these regions explains this enhanced corrosion.

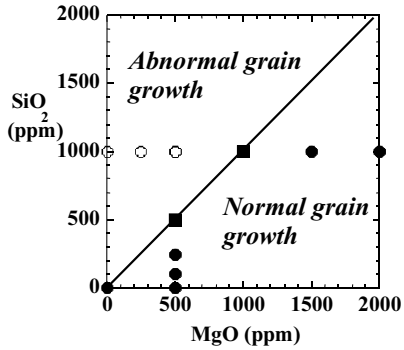

Figure 6 Critical Mg and Si doping concentrations for abnormal grain growth. The solid line represents the boundary for the onset of abnormal grain growth for samples sintered at 1650°C for 1 h. The open circles represent specimens in which abnormal grain growth was observed. The filled circles represent specimens in which no abnormal grain growth was observed. The filled square symbols represent specimens in which only limited abnormal grain growth was observed.

for the initiation of abnormal grain growth during alumina sintering. The figure shows that microstructures will contain normal grains for Si/Mg concentration ratios less than unity, and abnormal grains for Si/Mg ratios greater than unity. Points on the plot are experimental observations. Samples with equimolar Si and Mg additions (i.e., 500 ppm Mg/500 ppm Al and 1000 ppm Mg/1000 ppm Al) are at the boundary between abnormal and normal grain morphologies. These transition samples primarily have uniaxial, normal grains with occasional inclusions of abnormal grains. The 45° line on the plot between normal and abnormal morphology in Fig. 6 reflects the underlying defect-compensation mechanism that determines segregation and mutual solid solubility shown as Equation 1. It is acknowledged that other glass-modifying impurity or dopant ions, such as Ca, can markedly alter the critical silica concentrations for the initiation of abnormal grain growth [23]. As such, the boundary line drawn in Fig. 6 may be shifted with different levels of background impurities.

We have reported elsewhere that Mg additions to Si-doped alumina cause a redistribution of segregated Si from grain boundaries into the bulk alumina lattice [16]. This increased solid solubility is believed to result from a defect compensation reaction:

$$\mathrm{MgO} + \mathrm{SiO_2} \xrightarrow{\mathrm{Al_2O_2}} \mathrm{Mg'_{Al}} + \mathrm{Si^{\bullet}_{Al}} + 3\mathrm{O^{\times}_{O}} \quad (1a)$$

$$\mathrm{Mg'_{Al}} + \mathrm{Si^{\bullet}_{Al}} + 3\mathrm{O^{\times}_{O}} \longrightarrow [\mathrm{Mg'_{Al}} - \mathrm{Si^{\bullet}_{Al}}]^{\times} + 3\mathrm{O^{\times}_{O}} \quad (1b)$$

The redistribution of Si and Mg from grain boundaries to the lattice and the current observations that equimolar codoping suppresses abnormal grain growth indicate that the important function of MgO as a sintering aid is to act as a "scavenger" that mitigates the deleterious effect of siliceous grain boundary phases on microstructure evolution. Once glassy films are eliminated, the resulting segregation behavior acts to control grain growth through either solute drag or solute redistribution. This redistribution also stabilizes the microstructure against initiation of further abnormal grains. The next section discusses the effect of solute redistribution on grain growth kinetics.

3.4. Grain growth kinetics

An equilibrium grain boundary dopant concentration has significant implications to the underlying mechanisms controlling grain growth kinetics. The most significant implication is that dopant redistribution must occur with changes in grain scale in order to maintain local equilibrium. Transport of these dopants during redistribution will be rate limiting under certain conditions. Different grains within the same sample can have quite different individual histories of change during sample annealing. Some grains may grow considerably larger than others. However, the equilibrium concentration of dopants at grain boundaries is similar for all grains independent of length and sintering history. A statistically significant number of grain boundaries have been analyzed by HRI-SIMS in samples doped singly with MgO or SiO_2.

The thermodynamic driving force for redistribution can be expressed in terms of the local chemical potential gradients [24]. At the equilibrium dopant concentration, the chemical potential of a dopant at a grain boundary, μ_{GB}, is equal to the chemical potential of the dopant in the second phase, $\mu_{\mathrm{second\,phase}}$:

$$\mu_{\mathrm{GB}} = \mu_{\mathrm{second\,phase}} \quad (2)$$

Under the driving force of grain boundary curvature, the grains coarsen and reduce the interfacial area thus raising the grain boundary dopant level above its local equilibrium concentration. This increases the chemical potential of the grain boundary, which results in a thermodynamic imbalance (gradient), between the dopant at grain boundaries and the same dopant in second phase sink:

$$\mu_{\mathrm{GB}} > \mu_{\mathrm{second\,phase}} \quad (3)$$

For the system to return to thermodynamic equilibrium, it requires an equalization of the chemical potentials of the dopants at grain boundaries and the same ions in the second phase sinks. The alumina system can return to thermodynamic equilibrium by redistributing the excess amount of dopant from the grain boundaries to second phase sinks where it accumulates and coarsens the sinks. Local differences in the chemical potentials provide the driving force for redistribution, which proceeds until the chemical potentials are equal.

Another way to reduce the dopant concentration at grain boundaries is by increasing the surface area of the grain boundary (i.e., by decreasing grain size). This means that excess dopant at grain boundaries acts against coarsening and, thus can considerably reduce grain boundary mobility and microstructure coarsening, providing that transport of the dopant from sources to sinks is rate limiting. In the case when dopant diffusion along grain boundaries is slow compared to the diffusion of aluminum and oxygen, the redistribution of excess dopant from grain boundaries to a second phase

sink will be the rate limiting step. In such a case, the kinetic time interval, dt, required for a system to redistribute an excess concentration of a dopant at a grain boundary, dC_{dopant}, will depend on the average distance between second phase sinks, l_{sinks}, and the diffusion rate of the dopant along grain boundaries, D_{dopant}

$$\frac{dC_{dopant}}{dt} = \frac{D_{dopant}}{l_{sinks}} \tag{4}$$

The excess dopant concentration, dC_{dopant}, can be expressed in terms of the change, dG, in the average grain size, G:

$$dC_{dopant} \propto G\,dG \tag{5}$$

Assuming a constant dopant diffusion rate:

$$D_{dopant} = \text{constant} \tag{6}$$

and assuming that the distance between the second phase sinks scales as the average grain size:

$$l_{sinks} \propto G \tag{7}$$

Substituting for D_{dopant} and l_{sinks} in Equation 4 and expressing the equation in terms of the grain size dependence:

$$\frac{dG}{dt} = D_{dopant}\left(\frac{1}{G}\right)^2 \tag{8}$$

On integration Equation 8 yields cubic kinetics for microstructure evolution:

$$G^3 - G_o^3 = D_{dopant}t \tag{9}$$

Coarsening is therefore strongly dependent on impurity diffusivity. Note that it is possible to derive several different kinetic laws depending on the various scale dependencies that may arise from considerations of constant segregant concentration. For example, if the dopant concentration is well below the solid solubility limit, grain growth will not be controlled by redistribution and one grain scale dependence will be lost. However, cubic kinetics are often observed for singly doped aluminas [9, 10, 24] and are considered here.

4. Conclusions

Magnesia segregates uniformly to grain boundaries of different scale in singly MgO-doped samples. The uniform segregation suggests a local equilibrium segregant concentration and implies that a significant redistribution of magnesia from grain boundaries to sinks, such as spinel, occurs during grain coarsening. Silica segregates uniformly to grain boundaries of abnormal grains of varying scale in singly SiO_2-doped samples. This again suggests that there is an equilibrium grain boundary concentration of silica similar to the case of singly MgO-doped alumina. The silica is believed to form an equilibrium thickness glassy grain boundary phase. Significant redistribution of the glassy phase from boundary regions to sinks, such as pores, occurs during coarsening. SIMS imaging of alumina samples codoped with MgO and SiO_2 provides direct evidence for an increase in MgO and SiO_2 mutual solubility. Corresponding changes in the grain morphology from a bimodal distribution, with abnormal plate-like grains typical for ceramics sintered in a presence of liquid grain boundary films, to a more uniform grain morphology also suggests removal of glassy films from the intergranular region. Codoping alumina with MgO in concentrations greater than SiO_2 suppresses abnormal grain growth. Uniform abnormal grain growth was observed throughout a sample when the SiO_2 concentration was greater than the MgO concentration. Suppression of abnormal grain growth results from the removal of glassy grain boundary phases on codoping. Dopant redistribution during coarsening may have a significant influence on grain growth kinetics.

Acknowledgments

We thank Dan Schaeffer (DuPont) for experimental assistance. Rowland Cannon (LBL) and Carol Handwerker (NIST) are acknowledged for stimulating discussions. This work was supported by the NSF under award DMR-9625354 and through the MRSEC program under NSF award DMR-9400379.

References

1. R. L. COBLE, *J. Appl. Phys.* **32**(5) (1961) 793.
2. *Idem.*, "Transparent Alumina and Method of Preparation," US Patent no. 3,026,210 (1962).
3. M. F. YAN, *Mater. Sci. Eng.* **48** (1981) 53.
4. S. J. BENNISON and M. P. HARMER, in "Ceramic Transactions," Vol. 7, edited by C. A. Handwerker, J. E. Blendell and W. A. Kaisser (The American Ceramic Society, Westerville, OH, USA, 1990) p. 13.
5. W. A. KAISSER, M. SPRISSLER, C. A. HANDWERKER and J. E. BLENDELL, *J. Amer. Ceram. Soc.* **70**(5) (1987) 339.
6. P. F. BECHER, *ibid.* **74**(2) (1991) 255.
7. R. L. COBLE and J. E. BURKE, *Prog. Ceram. Sci.* **3** (1963) 197.
8. P. CHANTIKUL, S. J. BENNISON and B. R. LAWN, *J. Amer. Ceram. Soc.* **73**(8) (1990) 2419.
9. S. J. BENNISON and M. P. HARMER, *ibid.* **66**(5) (1983) C90.
10. *Idem.*, *ibid.* **68**(1) (1985) C22.
11. R. LEVI-SETTI, J. M. CHABALA, K. L. GAVRILOV, R. MOGILEVSKY and K. K. SONI, *Scanning Microscopy* **7**(4) (1993) 1161.
12. J. M. CHABALA, K. K. SONI, J. LI, K. L. GAVRILOV and R. LEVI-SETTI, *Intern. J. Mass Spectrom. and Ion Proc.* **143** (1995) 191.
13. K. K. SONI, A. M. THOMPSON, M. P. HARMER, D. B. WILLIAMS, J. M. CHABALA and R. LEVI-SETTI, *J. Appl. Phys.* **66**(21) (1995) 2795.
14. A. M. THOMPSON, M. P. HARMER, D. B. WILLIAMS, K. K. SONI, J. M. CHABALA and R. LEVI-SETTI, in "Sintering Technology" (Marcel Dekker, New York, 1996) p. 309.
15. A. M. THOMPSON, K. K. SONI, H. M. CHAN, M. P. HARMER, D. B. WILLIAMS, J. M. CHABALA and R. LEVI-SETTI, *J. Amer. Ceram. Soc.* **80**(2) (1997) 373.
16. K. L. GAVRILOV, S. J. BENNISON, K. R. MIKESKA, J. M. CHABALA and R. LEVI-SETTI, *ibid.* **82**(4) (1999) 1001.

17. S. J. BENNISON and K. R. MIKESKA, US Patent no. 5,411,583 May (1995).
18. K. R. MIKESKA, S. J. BENNISON and S. L. GRICE, *J. Amer. Ceram. Soc*. **83**(5) (2000) 1160.
19. D. R. CLARKE, *ibid*. **70**(1) (1987) 15.
20. R. BRYDSON, S.-C. CHEN, F. L. RILEY, S. J. MILNE, X. PAN and M. RÜHLE, *ibid*. **81**(2) (1998) 369.
21. C. A. BATEMAN, S. J. BENNISON and M. P. HARMER, *ibid*. **72**(7) (1989) 1241.
22. C. A. HANDWERKER, P. A. MORRIS and R. L. COBLE, *ibid*. **72**(1) (1989) 130.
23. S. I. BAE and S. BAIK, *ibid*. **76**(4) (1993) 1065.
24. M. F. YAN, R. M. CANNON and H. K. BOWEN, "Ceramic Microstructure '76" (West-View Press, 1977) p. 276.

Received 4 December 2002
and accepted 5 June 2003